

Ternary fission analysis of $^{242,258}\text{Fm}$ nuclei using equatorial and collinear cluster tripartition configurations

Nitin Sharma, Amandeep Kaur ^{*}, and Manoj K. Sharma

School of Physics and Materials Science, Thapar Institute of Engineering and Technology, Patiala 147004, Punjab, India



(Received 28 August 2021; revised 6 January 2022; accepted 11 March 2022; published 5 April 2022)

The quantum mechanical fragmentation theory-based three cluster model is employed to investigate the ground-state ternary fission of two Fm isotopes nuclei having atomic mass $A_p = 242$ and 258. The mass asymmetry coordinate and the relative separation among the decaying fragments play a crucial role for the estimation of the fragmentation structure and related barrier penetration process. First, the choice of third fragment (A_3) is fixed by minimizing the probable A_3 fragments having different proton neutron configurations. Further, the fission fragment combinations ($A_1 + A_2 + A_3$) are identified for the fixed third fragments by selecting the channel of lower ternary fragmentation potential and higher relative fission yield. Two type of tripartition of radioactive nuclei are considered such as equatorial cluster tripartition (ECT) and collinear cluster tripartition (CCT). A comparative analysis of ternary fragmentation potential and relative fission yield within ECT and CCT geometrical arrangement is carried out for different choices of third fragment, i.e., $A_3 = 1$ to $A_p/3$. The choice of most probable fragments suggest that the proton and neutron magic shell closures play essential role in the ternary mass division. Finally, a relative analysis of binary and ternary fragmentation is worked out for better insight of dynamics involved.

DOI: [10.1103/PhysRevC.105.044602](https://doi.org/10.1103/PhysRevC.105.044602)

I. INTRODUCTION

A branch of nuclear physics, which explores the spontaneous emission of mass and energy from an unstable nucleus, is known as radioactivity [1]. Generally, radioactivity involves the alpha- (α), beta- (β), and gamma- (γ) decay processes. However, there may be a possibility of cluster radioactivity, heavy-particle radioactivity, and spontaneous fission (SF) decay channels depending on the shape, size, and internucleon forces of the radioactive element [2–4]. Among the aforementioned decay channels, SF is considered as a powerful tool that determines the stability of heavy and superheavy nuclei together with related structure aspects.

The SF process of actinides is expected to provide further insight of stability and dynamical evolution of radioactive nuclei [5–7]. Various studies suggest that nuclei belonging to actinide mass region generally exhibit asymmetric fission. However, the experimental analysis of Refs. [8,9] show that the isotopes of Fm exhibit a transition from asymmetric to symmetric fission in region of mass $A = 256$ to 258. In reference to this observation, recently, we have explored [10] the binary fission of $^{242-260}\text{Fm}$ isotopes with the inclusion of deformation and orientation effects in the framework of preformed cluster model (PCM). It was observed that potential energy surfaces and fission fragment mass distributions significantly depend on the mass of fissioning nuclei. In continuation of this work, here we intend to explore the

ternary fission (TF) of Fm isotopes of extreme masses such as $A = 242$ and 258. Usually, a binary fission mode comprises the emergence of two fragments of comparable masses, but some findings [11–13] give the idea of splitting of a radioactive nucleus into three fragments and the process is termed TF. This was first observed by Alvarez *et al.* [11] in 1947 where long-range α particles were observed in the company of two fission fragments. The literature indicate that the actinides and transactinides may decay spontaneously into three partitions. However, the disintegration occurs mainly through light-particle accompanied fission (LPF) in which the mass of third particle is much smaller than other two fission fragments. The analysis of LPF mostly includes ^4He as a third fragment due to its high stability [14–17]. Apart from this, the other nuclei like $^{1,2,3}\text{H}$, $^{6,8}\text{He}$, $^{6,7,8,9}\text{Li}$, and $^{9,10}\text{Be}$ have been observed in the spontaneous TF [18–20]. Besides LPF, there is also a possibility of true ternary fission (TTF), i.e., the partitioning of nucleus into three fragments of comparable masses [21,22]. It is to be noted here that spontaneous TTF have not been observed experimentally but some relevant predictions has been made in past. On the other hand, an experimental signature of TTF exists in the induced reactions where isotopes of C, N, O, F, Ne, Na, Mg, S, Al, Si, Ca, Mn, and Ni were measured as a heavier third fragment [23–27].

In the ternary fission, a fissioning nucleus may divide into three parts by following equatorial cluster tripartition (ECT) or collinear cluster tripartition (CCT). The process in which third fragment emission happens in a direction perpendicular to the fission axis is termed as equatorial or orthogonal emission as shown in Fig. 1(a). On the other hand, the configuration where the third fragment emits in the direction of fission axis is known as collinear or polar emission,

^{*}Present address: Department of Physics, Faculty of Science, University of Zagreb, Bijenička c.32, Zagreb-10000, Croatia; amanganday@gmail.com

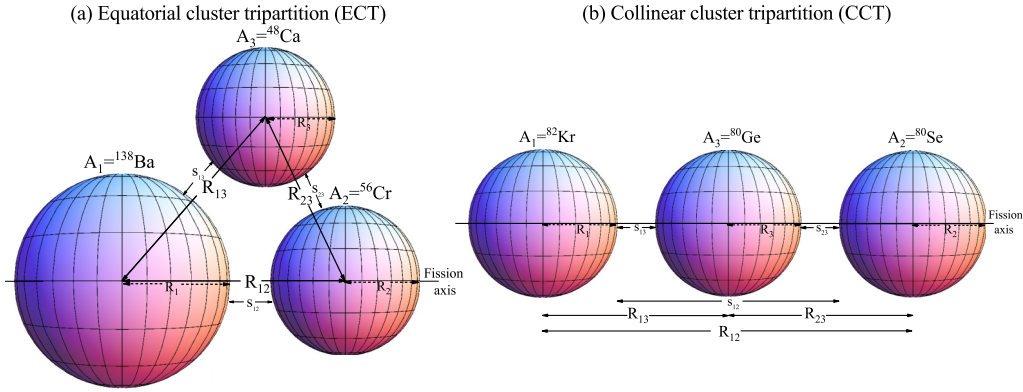


FIG. 1. (a) ECT and (b) CCT configurations of three spherical nuclei in the ternary fission decay. R_{ij} ($=R_i + R_j + s_{ij}$) is the distance between the center of two nuclei and s_{ij} is the surface separation distance between two nuclei. Here $i = 1, 2$ and $j = 2, 3$, where 1, 2, 3 correspond to the first, second, and third decay fragments, see Refs. [28,29].

see Fig. 1(b) [28,29]. Previously, some findings concluded that ECT is suited for the light-particle-accompanied fission, whereas CCT mode is better for the emission of heavier third fragment [29]. This work is devoted to analyze the ternary fragmentation behavior of $^{242,258}\text{Fm}$ radioactive nuclei involving wide range of light and heavy mass third fragments by employing ECT and CCT configurations.

In view of the above discussion, the present manuscript is devoted to fulfill the following objectives within the quantum mechanical theory-based (QMFT) [30–32] cluster decay models [10,15,29,33,34]: (i) the selection of third fragment by minimizing all possibilities of third fragments with respect to their charge numbers for $^{242,258}\text{Fm}$ parent nuclei; (ii) the impact of equatorial and collinear tripartition modes will be analyzed by studying the valleys of ternary fragmentation potential and peaks of relative fission yield; (iii) the identification of most probable nascent fission fragments, i.e., $A_1 + A_2 + A_3$; and (iv) a relative analysis of binary and ternary fission mass distributions.

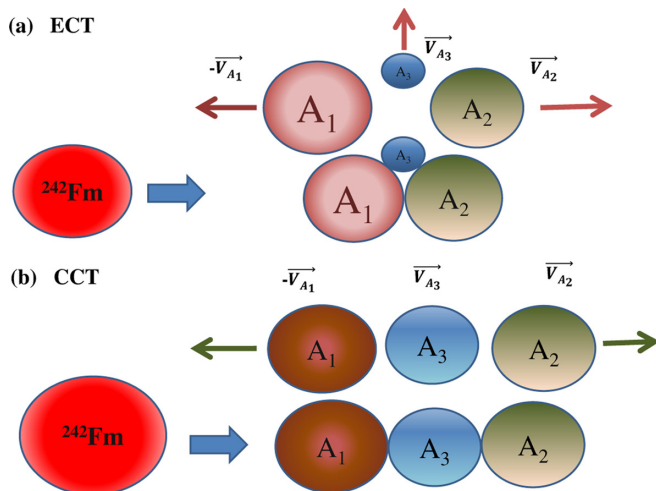


FIG. 2. A pictorial representation depicting the direction of the decay fragments in (a) ECT and (b) CCT configurations.

The overview of this manuscript is as follows. Section II describes the methodology. The QMFT-based PCM and three-cluster model (TCM) are employed to analyze the binary and ternary decay processes. The behavior of fragmentation potential and fission yield is studied in Sec. III using equatorial and collinear configuration. Note that all the calculations have been made using spherical choice of fragments only. Finally, the summary of the observed results is concluded in Sec. IV.

II. METHODOLOGY

The binary and ternary fission analysis is carried out within the framework of quantum mechanical fragmentation theory-based [30–32] PCM [10,34] and TCM [15,29,33]. This methodology is worked out in terms of the mass and charge asymmetry coordinates which represent the mass and charge flow, and read as

$$\eta_A = \frac{A_1 - A_2}{A_1 + A_2} \left(\text{and } \eta_Z = \frac{Z_1 - Z_2}{Z_1 + Z_2} \right). \quad (1)$$

In the above equation, the subscripts 1 and 2 denote the light and heavy fragments. In case of ternary fission, the third fragment represented by A_3 is kept fixed, and hence the mass and charge asymmetry is minimized in reference to A_1 and A_2 fragments. In addition to these coordinates, the model relies on the relative separation (R) between the decaying fragments. A brief description of PCM and TCM is given in the next sections.

A. Preformed cluster model

In PCM [10,34], the decaying fragment is supposed to be performed inside the radioactive nucleus and this formulation successfully addresses various spontaneous decay phenomena. The estimation of most probable decaying fragments in PCM is given by fragmentation potential and cluster preformation probability. The two-body fragmentation potential in PCM is given as

$$V_R(\eta) = \sum_{i=1}^2 B(A_i, Z_i) + V_C + V_p, \quad (2)$$

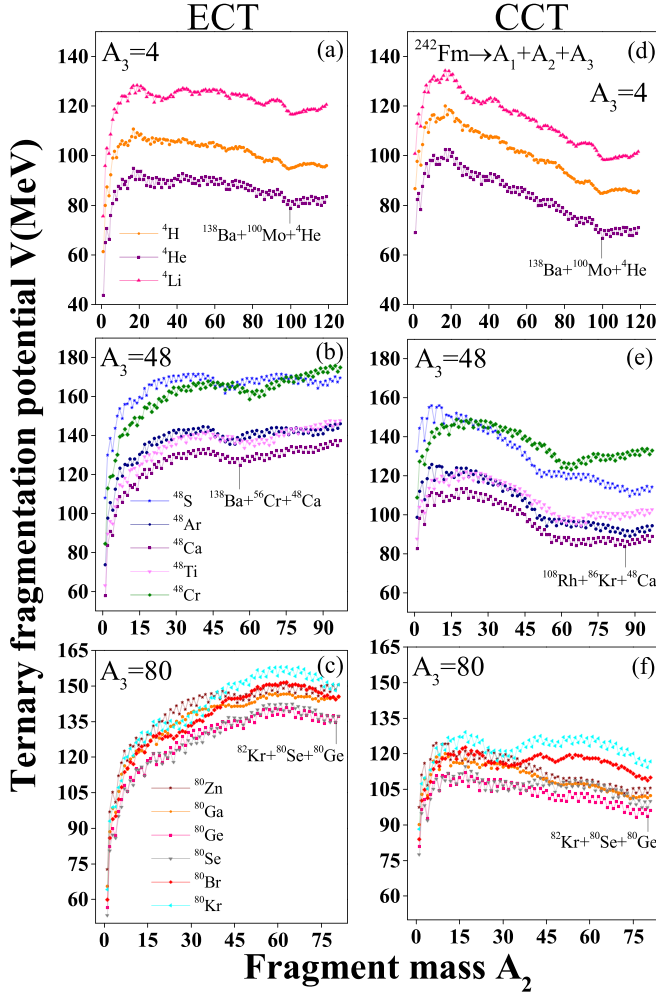


FIG. 3. Ternary fragmentation potential V (A_2) is calculated for different third fragments with mass number $A_3 = 4, 48,$ and 80 for ^{242}Fm radioactive nucleus using [(a)–(c)] ECT and [(d)–(f)] CCT emission modes.

where B_i , V_c , and V_p represent the binding energies, Coulomb potential, and nuclear potential; for details see Ref. [10]. In this model, the preformation probability is the solution of mass asymmetry-dependent Schrödinger equation, and penetrability is calculated using WKB approximation, for detailed description please refer to Refs. [10,34].

B. Three cluster model

TCM is an extension of PCM, where three-body decay phenomenon is studied in terms of η and R coordinates [29,33]. Using these coordinates, the three-body fragmentation potential V_{tot} reads as

$$V_{\text{tot}} = \sum_{i=1}^3 \sum_{j>i}^3 B_i + V_{Cij} + V_{Pij}. \quad (3)$$

The first term B_i represents the binding energy of fragments and calculated by the summation of macroscopic liquid drop model term V_{LDM} and the microscopic shell correction term δU , taken from the experimental findings of Audi and Wapstra

[35] or the theoretical estimates of Möller *et al.* [36] whenever not available in Ref. [35]. The Coulomb interaction V_{Cij} among three fragments is calculated using following relation [33]:

$$V_{Cij} = \frac{Z_i Z_j e^2}{R_{ij}}. \quad (4)$$

The interfragment distance R_{ij} or the relative separation among the fragments depends on the opted mode of the configuration such as *equatorial* or *collinear* [29], which is explained in the further discussion. The third term V_p in the fragmentation potential V_{tot} is the nuclear attractive proximity potential. In present work proximity 2000 (called as prox00) [37,38] potential is used for the calculations, where nuclear radii and the surface charge coefficients are given using the well-known droplet model concept:

$$V_p = 4\pi \bar{R} \gamma b \Phi(\xi). \quad (5)$$

The matter radius C_i reads as

$$C_i = c_i + (N_i/A_i)t_i, \quad (6)$$

where c_i denotes half-density radii of the charge distribution and t_i represents the neutron skin of the mother nucleus. The nuclear charge radius R_{00} (fm) be given as

$$R_{00i} = \sqrt{\frac{5}{3}} < r^2 >^{1/2} \quad (7)$$

$$= 1.240A_i^{1/3} \left(1 + \frac{1.646}{A_i} - 0.191 \frac{A_i - 2Z_i}{A_i} \right). \quad (8)$$

The half-density radius c_i can be obtained from the relation [37]

$$c_i = R_{00i} \left(1 - \frac{7}{2} \frac{b^2}{R_{00i}^2} - \frac{49}{8} \frac{b^4}{R_{00i}^4} + \dots \right). \quad (9)$$

The neutron skin t_i is given as [37]

$$t_i = \frac{3}{2} r_0 \frac{J I_i - \frac{1}{12} c_1 Z_i A_i^{-1/3}}{q + \frac{9}{4} J A_i^{-1/3}}, \quad (10)$$

where $r_0 = 1.4$ fm, the energy constant $J = 32.65$ MeV, the constant $c_1 = (3/5)(e^2/r_0) = 0.757895$ MeV, and the neutron skin stiffness coefficient $q = 35.4$ MeV. The nuclear surface energy coefficient γ in terms of neutron skin can be written as

$$\gamma = \frac{1}{4\pi r_0^2} \left[18.63 \text{ (MeV)} - q \frac{t_1^2 + t_2^2}{2r_0^2} \right], \quad (11)$$

where t_1 and t_2 can be calculated using Eq. (10), and the universal function can be written as

$$\phi(\xi) = \begin{cases} -0.1353 + \sum_{i=0}^5 \frac{c_n}{n+1} (2.5 - \xi)^{n+1} & \text{for } 0 < \xi \leq 2.5 \\ -0.09551 \exp\left[\frac{2.75 - \xi}{0.7176}\right] & \text{for } \xi > 2.5 \end{cases}, \quad (12)$$

where $\xi = R - C_i - C_j$. The values of the constants c_n are as follows: $c_0 = -0.1886$, $c_1 = -0.2628$,

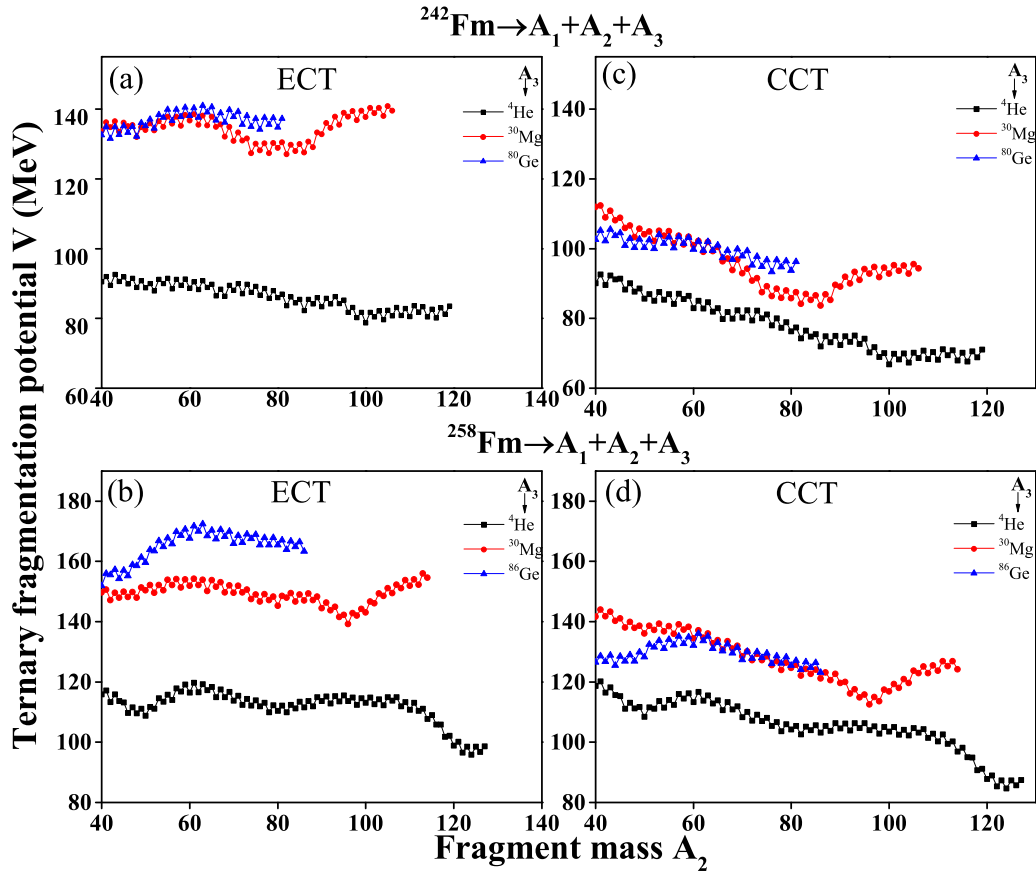


FIG. 4. Ternary fragmentation potential V (MeV) as a function of fragment mass A_2 for identified choices of third fragments for [(a) and (c)] ^{242}Fm and [(b) and (d)] ^{258}Fm nuclei using ECT and CCT configuration modes.

$c_2 = -0.15216$, $c_3 = -0.04562$, $c_4 = 0.069136$, and $c_5 = -0.011454$. The penetration probability of three-body decay channel to cross the potential barrier is estimated

$$P = \exp \left[-\frac{2}{\hbar} \int_{s_1}^{s_2} \{2\mu[V(R) - Q]\}^{1/2} ds \right]. \quad (13)$$

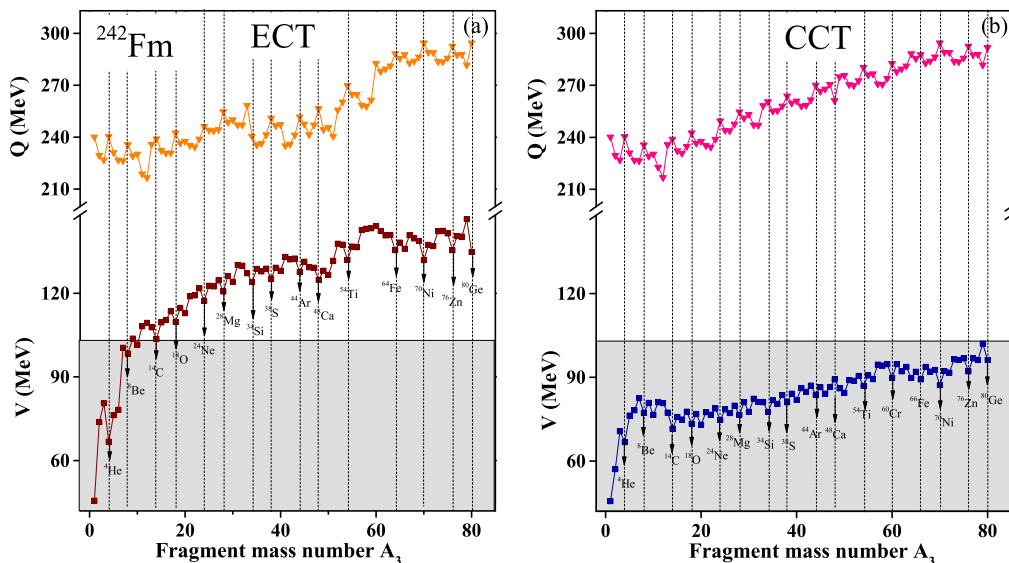


FIG. 5. The ternary fragmentation potential as a function of third fragment mass A_3 for ^{242}Fm using (a) equatorial and (b) collinear configuration modes.

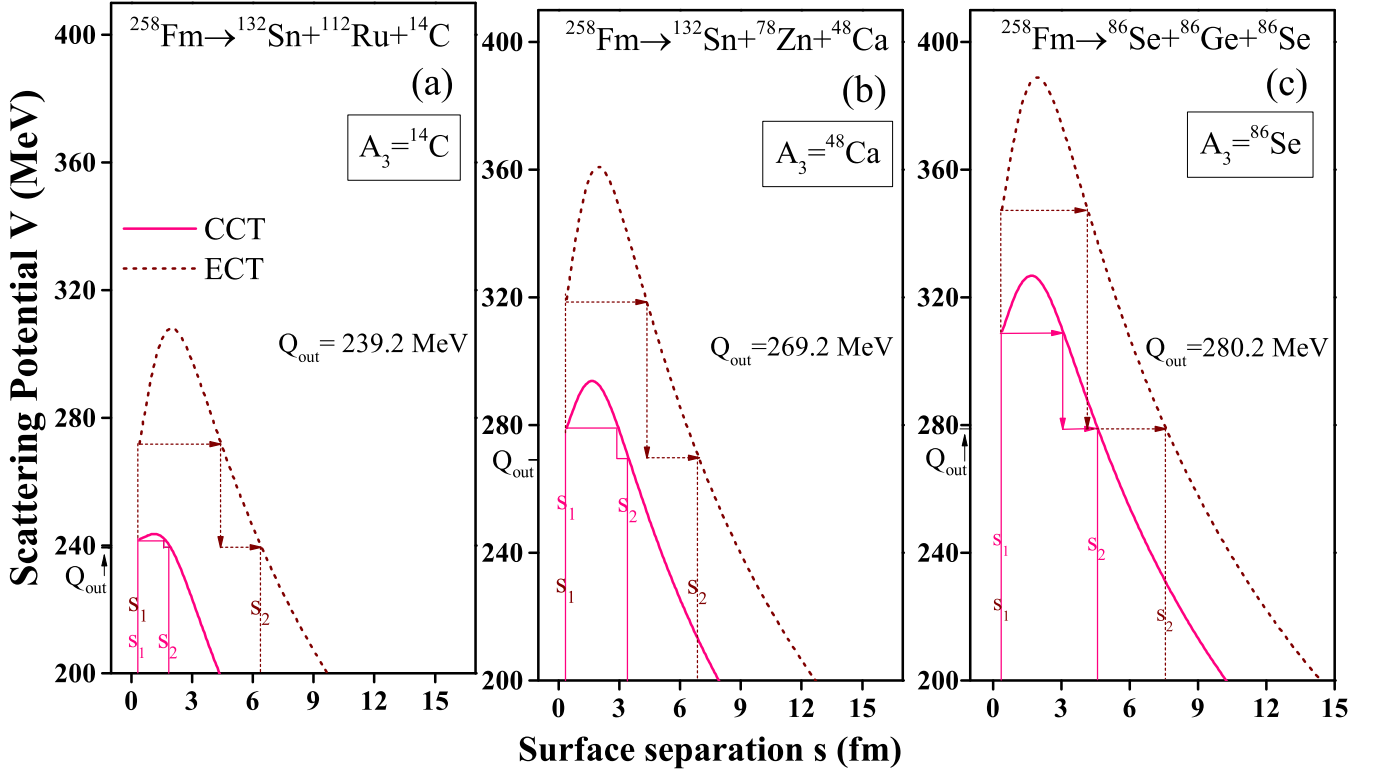


FIG. 6. The calculated scattering potential V (MeV) as a function of surface separation distance (s) for fixed third fragments such as (a) ^{14}C , (b) ^{48}Ca , and (c) ^{86}Se of ^{258}Fm for both ECT and CCT emission modes.

s_1 and s_2 are the first and second turning point satisfying the $V(s_2) = Q$ condition [can be seen in (Fig. 6)].

The Q value is assumed to be shared between three fragments ($Q = E_1 + E_2 + E_3$) and is obtained as $Q = M - \sum_{i=1}^3 m_i$. In CCT mode, most of the Q value is assumed to be shared between first and the second fragments and moving in opposite directions among the three decay products where as the third fragment is considered with negligible kinetic energy [39–41] and taken as rest [29]. A pictorial presentation depicting the direction of emitted fragments in ECT and CCT mode can be seen in Fig. 2. Initially, the fragments are considered to be in touching stage and then starts moving with common surface separation s . In Eq. (13), μ is the reduced mass of three fragments,

$$\mu_{123} = \left(\frac{\mu_{12}A_3}{\mu_{12} + A_3} \right) m, \quad (14)$$

where $\mu_{12} = A_1A_2/(A_1 + A_2)$ and m is the nucleon mass.

The relative yields for all the fragmentation channels for both binary [33] and ternary decay [29] processes are calculated as the ratio between the penetration probability of a given fragment over the sum of penetration probabilities of all possible fragmentation as

$$Y(A_i, Z_i) = \frac{P(A_i, Z_i)}{\sum P(A_i, Z_i)}. \quad (15)$$

The configuration mode where the third fragment emission happens orthogonally to the fission axis is known as equatorial configuration arrangement [29]. The pictorial representation

of equatorial configuration is given in Fig. 1(a). In this case, the relative separation in between the fragments is taken as [29]

$$R_{12} = R_1 + R_2 + s_{12}, \quad (16)$$

$$R_{23} = R_2 + R_3 + s_{23}, \quad (17)$$

$$R_{31} = R_3 + R_1 + s_{31}. \quad (18)$$

Here R_1 , R_2 , and R_3 represent the radius vector of three fragments, and the surface separation considered as

$$s_{12} = s_{23} = s_{31} = s. \quad (19)$$

On the other hand, the configuration mode where the third fragment emission happens along with the the fission axis is known as collinear configuration arrangement, see Fig. 1(b). The relative distance in between the center of fragments is taken as

$$R_{12} = R_1 + R_2 + s_{12}, \quad (20)$$

$$R_{23} = R_2 + R_3 + s_{23}, \quad (21)$$

$$R_{31} = R_3 + R_1 + s_{31}. \quad (22)$$

Here for collinear emission the surface separation

$$s_{12} = 2(R_3 + s), \quad s_{23} = s_{31} = s. \quad (23)$$

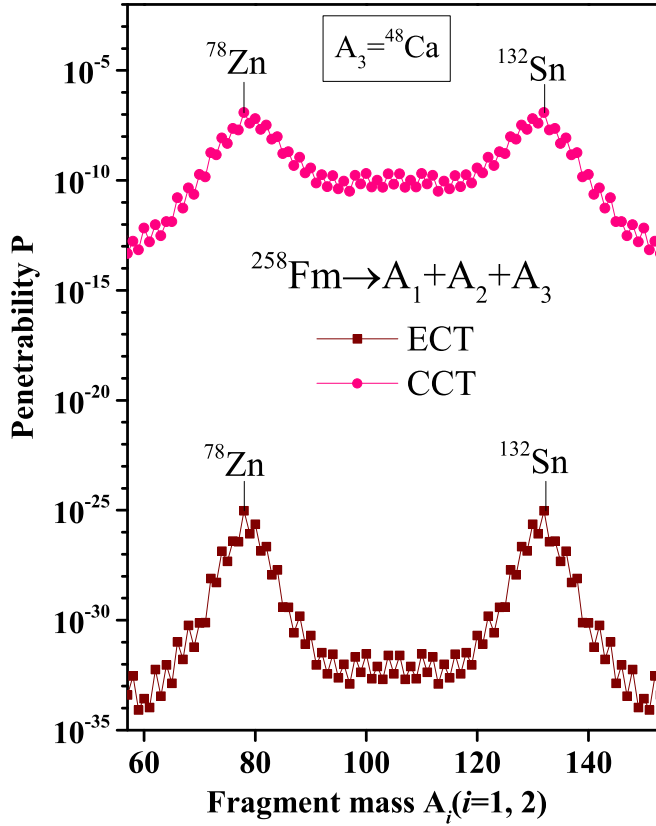


FIG. 7. Penetrability P as a function of A_i ($i = 1, 2$) of ^{258}Fm parent nucleus for $A_3 = ^{48}\text{Ca}$ to compare equatorial and collinear emission modes.

Note that in the present work, we have considered common surface separation $s = 0.4$ fm for which the barrier penetration works.

III. CALCULATIONS AND DISCUSSIONS

First, the third fragment (A_3) is selected by minimizing all possible third fragments with respect to their charge (Z) numbers. The TCM-calculated three-body fragmentation potential of ^{242}Fm fissioning nucleus for fixed mass numbers of third fragment $A_3 = 4, 48, \text{ and } 80$ is plotted in Figs. 3(a)–3(c) and Figs. 3(d)–3(f) for ECT and CCT configurations, respectively. These choices are taken to examine the behavior of fragmentation potential for lighter to heavier mass third fragments. For example, the fragment mass $A_3 = 4$ has three possibilities such as ^4H , ^4He , and ^4Li , leaving the remaining system as ^{238}Es , ^{238}Cf , and ^{238}Bk , respectively, whose binary fragmentation ($A_1 + A_2$) is properly minimized in the charge or mass asymmetry (η_Z) coordinate. Using these choices, the ternary fragmentation potential is calculated for the ^{242}Fm nucleus, see Figs. 3(a) and 3(d), and the lowest among these three is the most favorable A_3 fragment, i.e., ^4He for both ECT and CCT choices. We have 12 possible choices of charge number for both $A_3 = 48$ and 80 fragments such as ($Z = 16$ to 27) and ($Z = 29$ to 40). However, the ternary fragmentation potential is represented for the limited cases just for the clarity. It is noticed from figure that ^4He , ^{48}Ca , and ^{80}Ge are the most

preferred choices among their competing fragments due to the lower fragmentation potential independent of the choice of cluster tripartition configurations. Moreover, the magnitude and structure of fragmentation potential is significantly modified when one shifts from the ECT to CCT configuration. A similar analysis is carried out for the ^{258}Fm nucleus, but not shown here to avoid repetition, and it is observed that ^4He , ^{48}Ca , and ^{86}Se are the most favorable choices for the third fragment.

Further, the deepest minima in the fission region of the ternary fragmentation potential of the most favorable A_3 fragment are also marked with vertical line in Figs. 3(a)–3(f) for all considered cases. Interestingly, the choice of third fragment A_3 remains the same and independent of the type of the cluster tripartition; however, the most preferred $A_1 + A_2$ fragments can be different for ECT/CCT approaches.

Note that the deep valley of the fragmentation potential gives the most probable fission fragment combination as they are more stable than the neighboring decay fragments. It is observed that such kind of minima in the fragmentation structure is mainly due to the influence of shell closure effects of the fragment combination. As a consequence, lowest magnitude of fragmentation potential is observed for those fragments which have either magic proton/neutron numbers or lying in the neighborhood of magic shell closures. Therefore, the magic nuclide is observed as one or two of the decay fragments.

From Fig. 3, the identified most probable fission fragment combinations ($A_1 + A_2 + A_3$) for ECT mode are $^{138}\text{Ba}(Z = 56, N = 82) + ^{100}\text{Mo}(N = 58, Z = 42) + ^4\text{He}(Z = 2, N = 2)$, $^{138}\text{Ba}(Z = 56, N = 82) + ^{56}\text{Cr}(Z = 24, N = 32) + ^{48}\text{Ca}(Z = 20, N = 28)$, $^{82}\text{Kr}(Z = 34, N = 48) + ^{80}\text{Se}(Z = 34, N = 46) + ^{80}\text{Ge}(Z = 32, N = 48)$, and for CCT partition the fragment combination is same for $A_3 = ^4\text{He}$ and ^{80}Ge but different for $A_3 = ^{48}\text{Ca}$ as: $^{108}\text{Ru}(Z = 44, N = 64) + ^{86}\text{Kr}(Z = 36, N = 50) + ^{48}\text{Ca}(Z = 20, N = 28)$. This may happen because of the contribution of Coulomb potential, which reduces in the CCT configuration due to the large interfragment distance between A_1 and A_2 see Fig. 1(b), and this impact is high for heavier A_3 fragment.

Following the same procedure, the most preferred choices for third fragment from mass $A_3 = 1$ to $A_P/3$ are identified and listed in Tables I and II for ^{242}Fm and ^{258}Fm parent nuclei, respectively. Here A_P is the mass of parent nuclei. The fragment combinations ($A_1 + A_2 + A_3$) having the lowest value in the ternary fission region are also shown in the tables. Note that, a condition of $A_1 \geq A_2 \geq A_3$ is imposed in the calculations to avoid the repetition of fragment combination. It is observed that the choice of third fragment A_3 remains same and independent of the choice of tripartition, and in agreement with the results of Fig. 3. However, the most preferred $A_1 + A_2$ fragments get changed for many cases as listed Tables I and II. The proton and neutron numbers are also mentioned along with the fragment combination. The proton ($Z = 2, 8, 20, 28, \text{ and } 50$) and neutron ($N = 2, 8, 20, 28, 50, \text{ and } 82$) shell closures of all fragments are marked with the bold letters. It is important to mention that except for few cases, the fragment combinations associate themselves with the magic shell at least for one fragment of tripartition. This

TABLE I. The most preferred ternary fission fragment combination ($A_1 + A_2$) along with fixed third fragment (A_3) for ECT and CCT configuration of ^{242}Fm parent nucleus. The corresponding proton (Z) and neutron (N) number are also listed.

ECT		CCT	
Fragment combination	$(N_1, Z_1)+(N_2, Z_2)+(N_3, Z_3)$	Fragment combination	$(N_1, Z_1)+(N_2, Z_2)+(N_3, Z_3)$
$^{121}\text{Sn} + ^{120}\text{Sn} + ^1\text{n}$	(71, 50)+(70, 50)+(1,0)		
$^{138}\text{Ba} + ^{104}\text{Tc} + ^2\text{H}$	(82 ,56)+(61,43)+(1,1)		
$^{139}\text{La} + ^{100}\text{Mo} + ^3\text{H}$	(82 ,57)+(58,42)+(2,1)		
$^{138}\text{Ba} + ^{100}\text{Mo} + ^4\text{He}$	(82 ,56)+(58,42)+(2,2)		
$^{138}\text{Ba} + ^{99}\text{Mo} + ^5\text{He}$	(82 ,56)+(57,42)+(3,2)		
$^{138}\text{Ba} + ^{98}\text{Mo} + ^6\text{He}$	(82 ,56)+(56,42)+(4,2)		
$^{138}\text{Ba} + ^{97}\text{Nb} + ^7\text{Li}$	(82 ,56)+(56,41)+(4,3)		
$^{138}\text{Ba} + ^{96}\text{Zr} + ^8\text{Be}$	(82 ,56)+(56,40)+(4,4)		
$^{138}\text{Ba} + ^{95}\text{Zr} + ^9\text{Be}$	(82 ,56)+(55,40)+(5,4)		
$^{138}\text{Ba} + ^{95}\text{Zr} + ^{10}\text{Be}$	(82 ,56)+(55,40)+(6,4)		
$^{141}\text{Ba} + ^{90}\text{Y} + ^{11}\text{Be}$	(83,58)+(52,38)+(7,4)	$^{138}\text{Ba} + ^{93}\text{Zr} + ^{11}\text{Be}$	(82 ,56)+(53,40)+(7,4)
$^{140}\text{Ce} + ^{90}\text{Sr} + ^{12}\text{Be}$	(82 ,58)+(52,38)+(8,4)		
$^{138}\text{Ba} + ^{91}\text{Sr} + ^{13}\text{C}$	(82 ,56)+(53,38)+(7,6)		
$^{138}\text{Ba} + ^{90}\text{Sr} + ^{14}\text{C}$	(82 ,56)+(52,38)+(8,6)		
$^{138}\text{Ba} + ^{89}\text{Sr} + ^{15}\text{C}$	(82 ,56)+(51,38)+(9,6)		
$^{138}\text{Ba} + ^{88}\text{Sr} + ^{16}\text{C}$	(82 ,56)+(50,38)+(10,6)		
$^{139}\text{La} + ^{86}\text{Kr} + ^{17}\text{N}$	(82 ,57)+(50,36)+(10,7)	$^{137}\text{Cs} + ^{88}\text{Sr} + ^{17}\text{N}$	(82 ,55)+(50,38)+(10,7)
$^{138}\text{Ba} + ^{86}\text{Kr} + ^{18}\text{O}$	(82 ,56)+(50,36)+(10,8)		
$^{137}\text{Ba} + ^{86}\text{Kr} + ^{19}\text{O}$	(81,56)+(50,36)+(11,8)		
$^{136}\text{Ba} + ^{86}\text{Kr} + ^{20}\text{O}$	(80,56)+(50,36)+(12,8)		
$^{133}\text{Xe} + ^{88}\text{Sr} + ^{21}\text{O}$	(79,54)+(50,38)+(13,8)		
$^{132}\text{Xe} + ^{88}\text{Sr} + ^{22}\text{O}$	(78,54)+(50,38)+(14,8)		
$^{131}\text{I} + ^{88}\text{Sr} + ^{23}\text{F}$	(78,53)+(50,38)+(14,9)		
$^{132}\text{Xe} + ^{86}\text{Kr} + ^{24}\text{Ne}$	(78,54)+(50,36)+(14,10)	$^{132}\text{Te} + ^{88}\text{Sr} + ^{24}\text{Ne}$	(80,52)+(50,38)+(14,10)
$^{129}\text{Te} + ^{88}\text{Sr} + ^{25}\text{Ne}$	(77,52)+(50,38)+(15,10)		
$^{128}\text{Te} + ^{88}\text{Sr} + ^{26}\text{Ne}$	(76,52)+(50,38)+(16,10)		
$^{129}\text{I} + ^{86}\text{Kr} + ^{27}\text{Na}$	(76,53)+(50,36)+(16,11)	$^{127}\text{Sb} + ^{88}\text{Sr} + ^{27}\text{Na}$	(76,51)+(50,38)+(16,11)
$^{128}\text{Te} + ^{86}\text{Kr} + ^{28}\text{Mg}$	(76,52)+(50,36)+(16,12)		
$^{127}\text{Te} + ^{86}\text{Kr} + ^{29}\text{Mg}$	(75,52)+(50,36)+(17,12)	$^{124}\text{Sn} + ^{89}\text{Sr} + ^{29}\text{Mg}$	(74,50)+(51,38)+(17,12)
$^{126}\text{Te} + ^{86}\text{Kr} + ^{30}\text{Mg}$	(74,52)+(50,36)+(18,12)	$^{124}\text{Sn} + ^{88}\text{Sr} + ^{30}\text{Mg}$	(74,50)+(50,38)+(18,12)
$^{123}\text{Sn} + ^{88}\text{Sr} + ^{31}\text{Mg}$	(73,50)+(50,38)+(19,12)		
$^{122}\text{Sn} + ^{88}\text{Sr} + ^{32}\text{Mg}$	(72,50)+(50,38)+(20,12)		
$^{123}\text{Sn} + ^{86}\text{Kr} + ^{33}\text{Si}$	(73,50)+(50,36)+(19,14)		
$^{140}\text{Ce} + ^{68}\text{Ni} + ^{34}\text{Si}$	(82 ,58)+(40,28)+(20,14)	$^{122}\text{Sn} + ^{86}\text{Kr} + ^{34}\text{Si}$	(72,50)+(50,36)+(20,14)
$^{140}\text{Ce} + ^{67}\text{Ni} + ^{35}\text{Si}$	(82 ,58)+(39,28)+(21,14)	$^{121}\text{Sn} + ^{86}\text{Kr} + ^{35}\text{Si}$	(71,50)+(50,36)+(21,14)
$^{140}\text{Ce} + ^{66}\text{Ni} + ^{36}\text{Si}$	(82 ,58)+(38,28)+(22,14)	$^{120}\text{Sn} + ^{86}\text{Kr} + ^{36}\text{Si}$	(70,50)+(50,36)+(22,14)
$^{139}\text{La} + ^{66}\text{Ni} + ^{37}\text{P}$	(82 ,57)+(38,28)+(22,15)	$^{119}\text{In} + ^{86}\text{Kr} + ^{37}\text{P}$	(70,49)+(50,36)+(22,15)
$^{138}\text{Ba} + ^{66}\text{Ni} + ^{38}\text{S}$	(82 ,56)+(38,28)+(22,16)	$^{122}\text{Sn} + ^{82}\text{Se} + ^{38}\text{S}$	(72,50)+(48,34)+(22,16)
$^{137}\text{Ba} + ^{66}\text{Ni} + ^{39}\text{S}$	(81,56)+(38,28)+(23,16)	$^{121}\text{Sn} + ^{82}\text{Se} + ^{39}\text{S}$	(71,50)+(48,34)+(23,16)
$^{136}\text{Ba} + ^{66}\text{Ni} + ^{40}\text{S}$	(80,56)+(38,28)+(24,16)	$^{120}\text{Sn} + ^{82}\text{Se} + ^{40}\text{S}$	(70,50)+(48,34)+(24,16)
$^{140}\text{Ce} + ^{61}\text{Fe} + ^{41}\text{S}$	(82 ,58)+(35,26)+(25,16)	$^{115}\text{Cd} + ^{86}\text{Kr} + ^{41}\text{S}$	(67,48)+(50,36)+(25,16)
$^{139}\text{Tc} + ^{60}\text{Fe} + ^{42}\text{S}$	(82 ,58)+(34,26)+(26,16)	$^{114}\text{Cd} + ^{86}\text{Kr} + ^{42}\text{S}$	(66,48)+(50,36)+(26,16)
$^{139}\text{La} + ^{60}\text{Fe} + ^{43}\text{Cl}$	(82 ,57)+(34,26)+(26,17)	$^{113}\text{Ag} + ^{86}\text{Kr} + ^{43}\text{Cl}$	(66,47)+(50,36)+(26,17)
$^{138}\text{Ba} + ^{60}\text{Fe} + ^{44}\text{Ar}$	(82 ,56)+(34,26)+(26,18)	$^{112}\text{Pd} + ^{86}\text{Kr} + ^{44}\text{Ar}$	(66,46)+(50,36)+(26,18)
$^{137}\text{Ba} + ^{60}\text{Fe} + ^{45}\text{Ar}$	(81,56)+(34,26)+(27,18)	$^{111}\text{Pd} + ^{86}\text{Kr} + ^{45}\text{Ar}$	(65,46)+(50,36)+(27,18)
$^{140}\text{Ce} + ^{56}\text{Cr} + ^{46}\text{Ar}$	(82,58)+(32,24)+(28,18)	$^{110}\text{Pd} + ^{86}\text{Kr} + ^{46}\text{Ar}$	(64,46)+(50,36)+(28,18)
$^{139}\text{La} + ^{56}\text{Cr} + ^{47}\text{K}$	(82 ,57)+(32,24)+(28,19)	$^{109}\text{Rh} + ^{86}\text{Kr} + ^{47}\text{K}$	(64,45)+(50,36)+(28,19)
$^{138}\text{Ba} + ^{56}\text{Cr} + ^{48}\text{Ca}$	(82 ,56)+(32,24)+(28,20)	$^{108}\text{Ru} + ^{86}\text{Kr} + ^{48}\text{Ca}$	(64,44)+(50,36)+(28,20)
$^{141}\text{Ce} + ^{52}\text{Ti} + ^{49}\text{Ca}$	(83,58)+(30,22)+(29,20)	$^{107}\text{Ru} + ^{86}\text{Kr} + ^{49}\text{Ca}$	(63,44)+(50,36)+(29,20)
$^{140}\text{Ce} + ^{52}\text{Ti} + ^{50}\text{Ca}$	(82 ,58)+(30,22)+(30,20)	$^{106}\text{Ru} + ^{86}\text{Kr} + ^{50}\text{Ca}$	(62,44)+(50,36)+(30,20)
$^{140}\text{Ce} + ^{51}\text{Ti} + ^{51}\text{Ca}$	(82 ,58)+(29,22)+(31,20)	$^{105}\text{Ru} + ^{86}\text{Kr} + ^{51}\text{Ca}$	(61,44)+(50,36)+(31,20)
$^{124}\text{Te} + ^{66}\text{Ni} + ^{52}\text{Ca}$	(72,52)+(38,28)+(32,20)	$^{105}\text{Ru} + ^{86}\text{Kr} + ^{52}\text{Ca}$	(61,44)+(50,36)+(32,20)
$^{123}\text{Sb} + ^{66}\text{Ni} + ^{53}\text{Sc}$	(72,51)+(38,28)+(32,21)	$^{103}\text{Tc} + ^{86}\text{Kr} + ^{53}\text{Sc}$	(61,43)+(50,36)+(32,21)
$^{122}\text{Sn} + ^{66}\text{Ni} + ^{54}\text{Ti}$	(72,50)+(38,28)+(32,22)	$^{102}\text{Mo} + ^{86}\text{Kr} + ^{54}\text{Ti}$	(60,42)+(50,36)+(32,22)
$^{121}\text{Sn} + ^{66}\text{Ni} + ^{55}\text{Ti}$	(71,50)+(38,28)+(32,22)	$^{101}\text{Mo} + ^{86}\text{Kr} + ^{55}\text{Ti}$	(59,42)+(50,36)+(32,22)

TABLE I. (Continued.)

ECT		CCT	
Fragment combination	$(N_1, Z_1)+(N_2, Z_2)+(N_3, Z_3)$	Fragment combination	$(N_1, Z_1)+(N_2, Z_2)+(N_3, Z_3)$
$^{120}\text{Sn} + ^{66}\text{Ni} + ^{56}\text{Ti}$	$(70, \mathbf{50})+(38, \mathbf{28})+(34, 22)$	$^{100}\text{Mo} + ^{86}\text{Kr} + ^{56}\text{Ti}$	$(58, 42)+(50, 36)+(34, 22)$
$^{119}\text{Sn} + ^{66}\text{Ni} + ^{57}\text{Ti}$	$(69, \mathbf{50})+(38, \mathbf{28})+(35, 22)$	$^{99}\text{Mo} + ^{86}\text{Kr} + ^{57}\text{Ti}$	$(57, 42)+(50, 36)+(35, 22)$
$^{118}\text{Sn} + ^{66}\text{Ni} + ^{58}\text{Ti}$	$(68, \mathbf{50})+(38, \mathbf{28})+(36, 22)$	$^{98}\text{Mo} + ^{86}\text{Kr} + ^{58}\text{Ti}$	$(56, 42)+(50, 36)+(36, 22)$
$^{117}\text{In} + ^{66}\text{Ni} + ^{59}\text{V}$	$(68, 49)+(38, \mathbf{28})+(36, 23)$	$^{97}\text{Nb} + ^{86}\text{Kr} + ^{59}\text{V}$	$(56, 41)+(50, 38)+(37, 23)$
$^{96}\text{Zr} + ^{86}\text{Kr} + ^{60}\text{Cr}$	$(56, 40)+(50, 36)+(36, 24)$		
$^{91}\text{Sr} + ^{90}\text{Sr} + ^{61}\text{Cr}$	$(53, 38)+(52, 38)+(37, 24)$		
$^{90}\text{Sr} + ^{90}\text{Sr} + ^{62}\text{Cr}$	$(52, 38)+(52, 38)+(38, 24)$		
$^{90}\text{Sr} + ^{90}\text{Sr} + ^{63}\text{Mn}$	$(52, 38)+(52, 38)+(39, 24)$		
$^{90}\text{Sr} + ^{88}\text{Kr} + ^{64}\text{Fe}$	$(52, 38)+(50, 38)+(38, 24)$		
$^{91}\text{Sr} + ^{86}\text{Kr} + ^{65}\text{Fe}$	$(53, 38)+(50, 36)+(39, 26)$		
$^{91}\text{Sr} + ^{86}\text{Kr} + ^{65}\text{Fe}$	$(53, 38)+(50, 36)+(39, 26)$		
$^{90}\text{Sr} + ^{86}\text{Kr} + ^{66}\text{Fe}$	$(52, 38)+(50, 36)+(40, 26)$		
$^{89}\text{Sr} + ^{86}\text{Kr} + ^{67}\text{Fe}$	$(51, 38)+(50, 36)+(41, 26)$		
$^{88}\text{Sr} + ^{86}\text{Kr} + ^{68}\text{Fe}$	$(50, 38)+(50, 36)+(42, 26)$		
$^{87}\text{Rb} + ^{86}\text{Kr} + ^{69}\text{Co}$	$(50, 37)+(50, 36)+(42, 27)$		
$^{86}\text{Kr} + ^{86}\text{Kr} + ^{70}\text{Ni}$	$(50, 36)+(50, 36)+(42, 28)$		
$^{85}\text{Kr} + ^{86}\text{Kr} + ^{71}\text{Ni}$	$(49, 36)+(50, 36)+(43, 28)$		
$^{88}\text{Sr} + ^{82}\text{Se} + ^{72}\text{Ni}$	$(50, 38)+(48, 34)+(44, 28)$		
$^{88}\text{Sr} + ^{82}\text{Se} + ^{72}\text{Ni}$	$(50, 38)+(48, 34)+(44, 28)$		
$^{88}\text{Sr} + ^{81}\text{Se} + ^{73}\text{Ni}$	$(50, 38)+(47, 34)+(45, 28)$		
$^{88}\text{Sr} + ^{80}\text{Se} + ^{74}\text{Ni}$	$(50, 38)+(46, 34)+(46, 28)$		
$^{87}\text{Rb} + ^{80}\text{Se} + ^{75}\text{Cu}$	$(50, 37)+(46, 34)+(46, 29)$		
$^{86}\text{Kr} + ^{80}\text{Se} + ^{76}\text{Zn}$	$(50, 36)+(46, 34)+(46, 30)$		
$^{85}\text{Kr} + ^{80}\text{Se} + ^{77}\text{Zn}$	$(49, 36)+(46, 34)+(47, 30)$		
$^{84}\text{Kr} + ^{80}\text{Se} + ^{78}\text{Zn}$	$(48, 36)+(46, 34)+(48, 30)$		
$^{83}\text{Kr} + ^{80}\text{Se} + ^{79}\text{Zn}$	$(47, 36)+(46, 34)+(49, 30)$		
$^{82}\text{Kr} + ^{80}\text{Se} + ^{80}\text{Ge}$	$(48, 34)+(46, 34)+(48, 32)$		

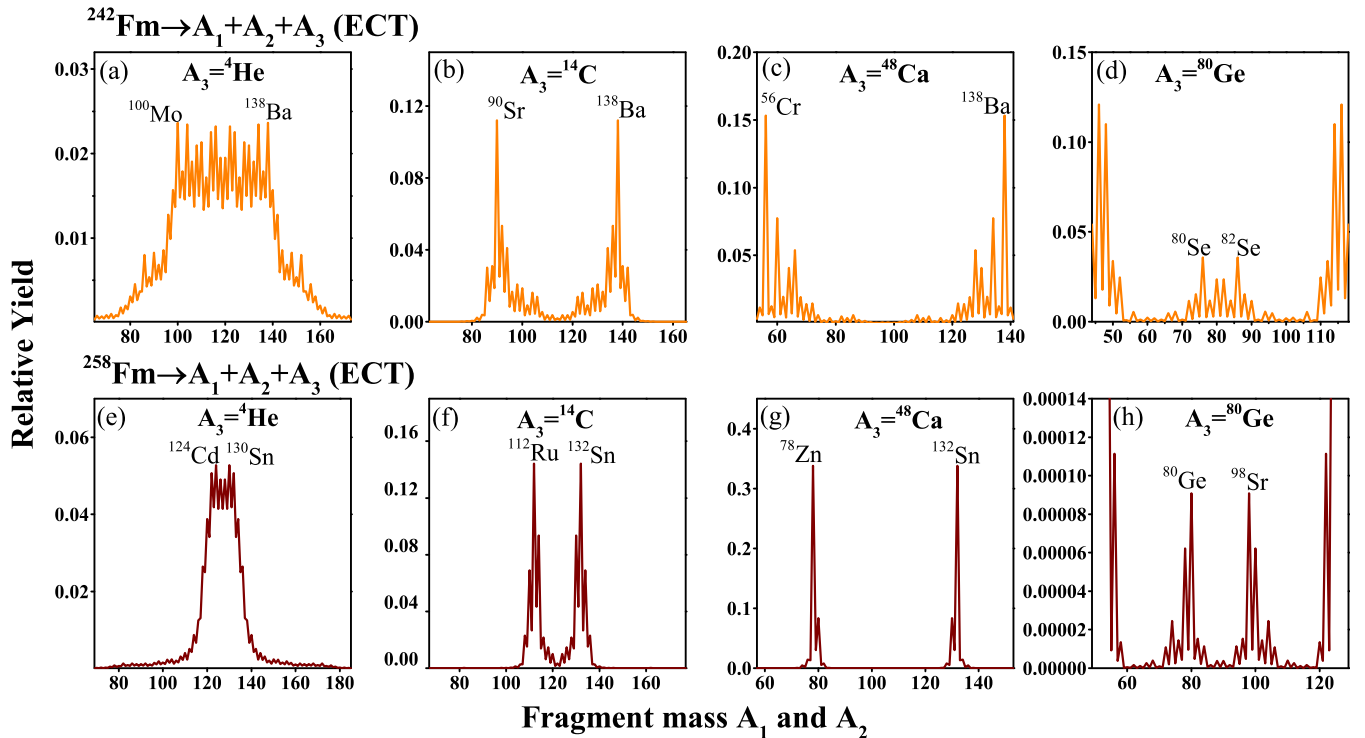


FIG. 8. The calculated relative fission yield as a function of fragment masses A_1 and A_2 for (a)–(d) ^{242}Fm and (e)–(h) ^{258}Fm for fixed A_3 fragments such as ^4He , ^{14}C , ^{48}Ca , and ^{80}Ge for ECT approach.

TABLE II. The most preferred ternary fission fragment combination ($A_1 + A_2$) along with fixed third fragment (A_3) for ECT and CCT configuration of ^{258}Fm parent nucleus. The corresponding proton (Z) and neutron (N) number are also listed.

ECT		CCT	
Fragment combination	$(N_1, Z_1)+(N_2, Z_2)+(N_3, Z_3)$	Fragment combination	$(N_1, Z_1)+(N_2, Z_2)+(N_3, Z_3)$
$^{129}\text{Sn} + ^{128}\text{Sn} + ^1\text{n}$	$(79,50)+(78,50)+(1,0)$		
$^{130}\text{Sn} + ^{126}\text{In} + ^2\text{H}$	$(80,50)+(77,49)+(1,1)$		
$^{130}\text{Sn} + ^{125}\text{In} + ^3\text{H}$	$(80,50)+(76,49)+(2,1)$		
$^{130}\text{Sn} + ^{124}\text{In} + ^4\text{He}$	$(80,50)+(76,48)+(2,2)$		
$^{131}\text{Sn} + ^{122}\text{Cd} + ^5\text{He}$	$(81,50)+(74,48)+(3,2)$		
$^{130}\text{Sn} + ^{122}\text{Cd} + ^6\text{He}$	$(80,50)+(74,48)+(4,2)$		
$^{132}\text{Sn} + ^{119}\text{Ag} + ^7\text{Li}$	$(82,50)+(72,47)+(4,3)$		
$^{132}\text{Sn} + ^{118}\text{Pd} + ^8\text{Be}$	$(82,50)+(72,46)+(4,4)$		
$^{131}\text{Sn} + ^{118}\text{Pd} + ^9\text{Be}$	$(81,50)+(72,46)+(5,4)$		
$^{132}\text{Sn} + ^{116}\text{Pd} + ^{10}\text{Be}$	$(82,50)+(70,46)+(6,4)$		
$^{131}\text{Sn} + ^{116}\text{Pd} + ^{11}\text{Be}$	$(81,50)+(70,46)+(7,4)$		
$^{130}\text{Sn} + ^{116}\text{Pd} + ^{12}\text{Be}$	$(80,50)+(70,46)+(8,4)$		
$^{132}\text{Sn} + ^{113}\text{Ru} + ^{13}\text{C}$	$(82,50)+(72,44)+(7,6)$		
$^{132}\text{Sn} + ^{112}\text{Ru} + ^{14}\text{C}$	$(82,50)+(72,44)+(8,6)$		
$^{131}\text{Sn} + ^{112}\text{Ru} + ^{15}\text{C}$	$(81,50)+(68,44)+(9,6)$		
$^{134}\text{Te} + ^{108}\text{Mo} + ^{16}\text{C}$	$(82,52)+(66,42)+(10,6)$		
$^{133}\text{Sb} + ^{108}\text{Mo} + ^{17}\text{N}$	$(82,51)+(66,42)+(10,7)$		
$^{132}\text{Sn} + ^{108}\text{Mo} + ^{18}\text{O}$	$(82,50)+(66,42)+(10,8)$		
$^{132}\text{Sn} + ^{107}\text{Mo} + ^{19}\text{O}$	$(82,50)+(65,42)+(11,8)$		
$^{132}\text{Sn} + ^{106}\text{Mo} + ^{20}\text{O}$	$(82,50)+(64,42)+(12,8)$		
$^{134}\text{Te} + ^{103}\text{Zr} + ^{21}\text{O}$	$(82,52)+(63,40)+(13,8)$	$^{131}\text{Sn} + ^{106}\text{Mo} + ^{21}\text{O}$	$(81,50)+(64,42)+(13,8)$
$^{134}\text{Te} + ^{102}\text{Zr} + ^{22}\text{O}$	$(82,52)+(62,40)+(14,8)$		
$^{133}\text{Sb} + ^{102}\text{Zr} + ^{23}\text{F}$	$(82,51)+(62,40)+(14,9)$		
$^{132}\text{Sn} + ^{102}\text{Zr} + ^{24}\text{Ne}$	$(82,50)+(62,40)+(14,10)$		
$^{132}\text{Sn} + ^{101}\text{Zr} + ^{25}\text{Ne}$	$(82,50)+(61,40)+(15,10)$		
$^{132}\text{Sn} + ^{100}\text{Zr} + ^{26}\text{Ne}$	$(82,50)+(60,40)+(16,10)$		
$^{133}\text{Sn} + ^{98}\text{Sr} + ^{27}\text{Na}$	$(82,50)+(60,38)+(16,11)$	$^{132}\text{Sn} + ^{99}\text{Y} + ^{27}\text{Na}$	$(82,50)+(60,39)+(16,11)$
$^{132}\text{Sn} + ^{98}\text{Sr} + ^{28}\text{Mg}$	$(82,50)+(60,38)+(16,12)$		
$^{132}\text{Sn} + ^{97}\text{Sr} + ^{29}\text{Mg}$	$(82,50)+(59,38)+(17,12)$		
$^{132}\text{Sn} + ^{96}\text{Sr} + ^{30}\text{Mg}$	$(82,50)+(58,38)+(18,12)$		
$^{131}\text{Sn} + ^{96}\text{Sr} + ^{31}\text{Mg}$	$(81,50)+(58,38)+(19,12)$		
$^{134}\text{Te} + ^{92}\text{Kr} + ^{32}\text{Mg}$	$(82,52)+(56,36)+(20,12)$	$^{132}\text{Sn} + ^{94}\text{Sr} + ^{32}\text{Mg}$	$(82,50)+(56,38)+(20,12)$
$^{132}\text{Sn} + ^{93}\text{Kr} + ^{33}\text{Si}$	$(82,50)+(57,36)+(19,14)$		
$^{132}\text{Sn} + ^{92}\text{Kr} + ^{34}\text{Si}$	$(82,50)+(56,36)+(20,14)$		
$^{132}\text{Sn} + ^{91}\text{Kr} + ^{35}\text{Si}$	$(82,50)+(55,36)+(21,14)$		
$^{134}\text{Te} + ^{88}\text{Se} + ^{36}\text{Si}$	$(82,52)+(54,34)+(22,14)$	$^{132}\text{Sn} + ^{90}\text{Kr} + ^{36}\text{Si}$	$(82,50)+(54,36)+(22,14)$
$^{133}\text{Sb} + ^{88}\text{Se} + ^{37}\text{P}$	$(82,51)+(54,34)+(22,15)$	$^{132}\text{Sn} + ^{89}\text{Br} + ^{37}\text{P}$	$(82,50)+(54,35)+(22,15)$
$^{132}\text{Sn} + ^{88}\text{Se} + ^{38}\text{S}$	$(82,50)+(54,34)+(22,16)$		
$^{132}\text{Sn} + ^{87}\text{Se} + ^{39}\text{S}$	$(82,50)+(53,34)+(23,16)$		
$^{132}\text{Sn} + ^{86}\text{Se} + ^{40}\text{S}$	$(82,50)+(52,34)+(24,16)$		
$^{134}\text{Te} + ^{83}\text{Ge} + ^{41}\text{S}$	$(82,52)+(51,32)+(25,16)$	$^{132}\text{Sn} + ^{85}\text{Se} + ^{41}\text{S}$	$(82,50)+(51,34)+(25,16)$
$^{134}\text{Te} + ^{82}\text{Ge} + ^{42}\text{S}$	$(82,52)+(50,32)+(26,16)$	$^{132}\text{Sn} + ^{84}\text{Se} + ^{42}\text{S}$	$(82,50)+(50,34)+(26,16)$
$^{133}\text{Sb} + ^{82}\text{Ge} + ^{43}\text{Cl}$	$(82,51)+(50,32)+(26,17)$	$^{132}\text{Sn} + ^{83}\text{As} + ^{43}\text{Cl}$	$(82,50)+(50,33)+(26,17)$
$^{132}\text{Sn} + ^{82}\text{Ge} + ^{44}\text{Ar}$	$(82,50)+(50,32)+(26,18)$		
$^{131}\text{Sn} + ^{82}\text{Ge} + ^{45}\text{Ar}$	$(81,50)+(50,32)+(27,18)$		
$^{134}\text{Te} + ^{78}\text{Zn} + ^{46}\text{Ar}$	$(82,52)+(48,30)+(28,18)$	$^{132}\text{Sn} + ^{78}\text{Zn} + ^{46}\text{Ar}$	$(82,50)+(48,30)+(28,18)$
$^{133}\text{Sb} + ^{78}\text{Zn} + ^{47}\text{K}$	$(82,51)+(48,30)+(28,19)$	$^{132}\text{Sn} + ^{79}\text{Ga} + ^{47}\text{K}$	$(82,50)+(57,32)+(28,19)$
$^{132}\text{Sn} + ^{78}\text{Zn} + ^{48}\text{Ca}$	$(82,50)+(48,30)+(28,20)$		
$^{131}\text{Sn} + ^{78}\text{Zn} + ^{49}\text{Ca}$	$(81,50)+(48,30)+(29,20)$		
$^{132}\text{Sn} + ^{76}\text{Zn} + ^{50}\text{Ca}$	$(82,50)+(46,30)+(30,20)$		
$^{131}\text{Sn} + ^{76}\text{Zn} + ^{51}\text{Ca}$	$(81,50)+(46,30)+(31,20)$		
$^{134}\text{Te} + ^{72}\text{Ni} + ^{52}\text{Ca}$	$(82,52)+(44,28)+(32,20)$	$^{130}\text{Sn} + ^{76}\text{Zn} + ^{52}\text{Ca}$	$(80,50)+(46,30)+(32,20)$
$^{133}\text{Sb} + ^{72}\text{Ni} + ^{53}\text{Sc}$	$(82,51)+(44,28)+(32,21)$	$^{132}\text{Sn} + ^{73}\text{Cu} + ^{53}\text{Sc}$	$(82,50)+(44,29)+(32,21)$
$^{132}\text{Sn} + ^{72}\text{Ni} + ^{54}\text{Ti}$	$(82,50)+(44,28)+(32,22)$		
$^{131}\text{Sn} + ^{72}\text{Ni} + ^{55}\text{Ti}$	$(81,50)+(44,28)+(33,22)$		

TABLE II. (Continued.)

ECT		CCT	
Fragment combination	$(N_1, Z_1)+(N_2, Z_2)+(N_3, Z_3)$	Fragment combination	$(N_1, Z_1)+(N_2, Z_2)+(N_3, Z_3)$
$^{132}\text{Sn} + ^{70}\text{Ni} + ^{56}\text{Ti}$	(82,50) +(42,28)+(34,22)		
$^{131}\text{Sn} + ^{70}\text{Ni} + ^{57}\text{Ti}$	(81,50)+(42,28)+(35,22)		
$^{130}\text{Sn} + ^{70}\text{Ni} + ^{58}\text{Ti}$	(80,50)+(42,28)+(36,22)		
$^{133}\text{Sb} + ^{66}\text{Fe} + ^{59}\text{V}$	(82,51) +(40,26)+(36,23)	$^{132}\text{Sn} + ^{67}\text{Co} + ^{59}\text{V}$	(82,50) +(40,27)+(36,23)
$^{132}\text{Sn} + ^{66}\text{Fe} + ^{60}\text{Cr}$	(82,50) +(40,26)+(36,24)		
$^{131}\text{Sn} + ^{66}\text{Fe} + ^{61}\text{Cr}$	(81,50)+(40,26)+(37,24)		
$^{130}\text{Sn} + ^{66}\text{Fe} + ^{62}\text{Cr}$	(80,50)+(40,26)+(38,24)	$^{132}\text{Sn} + ^{64}\text{Fe} + ^{62}\text{Cr}$	(82,50) +(38,26)+(38,24)
$^{132}\text{Sn} + ^{63}\text{Mn} + ^{63}\text{Mn}$	(82,50) +(38,25)+(38,25)		
$^{132}\text{Cd} + ^{66}\text{Fe} + ^{64}\text{Fe}$	(84,48)+(40,26)+(38,26)		
$^{127}\text{Cd} + ^{66}\text{Fe} + ^{65}\text{Fe}$	(79,48)+(40,26)+(39,26)		
$^{126}\text{Cd} + ^{66}\text{Fe} + ^{66}\text{Fe}$	(78,48)+(40,26)+(40,26)		
$^{124}\text{Cd} + ^{67}\text{Fe} + ^{67}\text{Fe}$	(76,48)+(41,26)+(41,26)	$^{109}\text{Mo} + ^{82}\text{Ge} + ^{67}\text{Fe}$	(67,42)+ (50,32) +(41,26)
$^{122}\text{Cd} + ^{68}\text{Fe} + ^{68}\text{Fe}$	(74,48)+(42,26)+(42,26)	$^{108}\text{Mo} + ^{82}\text{Ge} + ^{68}\text{Fe}$	(66,42)+ (50,32) +(42,26)
$^{108}\text{Mo} + ^{81}\text{Ga} + ^{69}\text{Co}$	(66,42)+(49,32)+(42,27)	$^{107}\text{Nb} + ^{82}\text{Ga} + ^{69}\text{Co}$	(66,41)+ (50,32) +(42,27)
$^{110}\text{Mo} + ^{78}\text{Zn} + ^{70}\text{Ni}$	(58,42)+(48,30)+(42,28)	$^{106}\text{Zr} + ^{82}\text{Ge} + ^{70}\text{Ni}$	(66,40)+ (50,32) +(42,28)
$^{109}\text{Mo} + ^{78}\text{Zn} + ^{71}\text{Ni}$	(57,42)+(48,30)+(43,28)	$^{105}\text{Zr} + ^{82}\text{Ge} + ^{71}\text{Ni}$	(65,40)+ (50,32) +(43,28)
$^{104}\text{Zr} + ^{82}\text{Ge} + ^{72}\text{Ni}$	(64,40)+ (50,32) +(44,28)		
$^{103}\text{Zr} + ^{82}\text{Ge} + ^{73}\text{Ni}$	(63,40)+ (50,32) +(45,28)		
$^{102}\text{Zr} + ^{82}\text{Ge} + ^{74}\text{Ni}$	(62,40)+ (50,32) +(46,28)		
$^{102}\text{Zr} + ^{81}\text{Ga} + ^{75}\text{Cu}$	(62,40)+ (50,31) +(46,29)	$^{101}\text{Y} + ^{82}\text{Ge} + ^{75}\text{Cu}$	(62,39)+ (50,32) +(46,29)
$^{102}\text{Zr} + ^{80}\text{Zn} + ^{76}\text{Zn}$	(62,40)+ (50,30) +(46,30)		
$^{103}\text{Zr} + ^{78}\text{Zn} + ^{77}\text{Zn}$	(63,40)+(48,30)+(47,30)	$^{99}\text{Sr} + ^{82}\text{Ge} + ^{77}\text{Zn}$	(61,38)+ (50,32) +(47,30)
$^{102}\text{Zr} + ^{78}\text{Zn} + ^{78}\text{Zn}$	(62,40)+(48,30)+(48,30)	$^{98}\text{Sr} + ^{82}\text{Ge} + ^{78}\text{Zn}$	(60,38)+ (50,32) +(48,30)
$^{97}\text{Sr} + ^{82}\text{Ge} + ^{79}\text{Zn}$	(59,38)+ (50,32) +(49,30)		
$^{98}\text{Sr} + ^{82}\text{Zn} + ^{80}\text{Ge}$	(60,38)+(52,30)+(48,32)	$^{96}\text{Kr} + ^{82}\text{Ge} + ^{80}\text{Ge}$	(60,36)+ (50,32) +(48,32)
$^{95}\text{Kr} + ^{82}\text{Ge} + ^{81}\text{Ge}$	(59,36)+ (50,32) +(49,32)		
$^{94}\text{Kr} + ^{82}\text{Ge} + ^{82}\text{Ge}$	(58,36)+ (50,32) +(50,32)		
$^{92}\text{Kr} + ^{83}\text{Ge} + ^{83}\text{Ge}$	(56,36)+(51,32)+(51,32)		
$^{88}\text{Se} + ^{86}\text{Se} + ^{84}\text{Ge}$	(54,34)+(52,34)+(52,32)		
$^{87}\text{Se} + ^{86}\text{Ge} + ^{85}\text{Se}$	(53,34)+(54,32)+(51,34)		
$^{86}\text{Se} + ^{86}\text{Ge} + ^{86}\text{Se}$	(52,34)+(54,32)+(52,34)		

result is in agreement with reference [42,43]. Interestingly, some of the predicted third fragments A_3 in Tables I and II are either observed or predicted in cluster radioactivity studies or in induced ternary fission [23–27,44,45].

CCT mode is observed experimentally for ^{252}Cf nucleus by Pyaktov *et al.* in 2010 [46] using the missing mass method. In this experiment $^{48-56}\text{Ca}$ is reported as the third fragment along with heavy Sn ($Z = 50$ magicity) as one of the fragment. In the present calculations, $^{48-52}\text{Ca}$ are emerged as third fragment in ECT as well as CCT mode for $^{242,258}\text{Fm}$ isotopes. The remaining fragments (fragment 1 and/or fragment 2) are reinforced via $Z = 50$ or $N = 82$ magicity as evident from Table I and II. Henceforth, the present calculations are in reasonable agreement with the experiment data [46].

Previous experimental studies of ternary fission have pointed out that the third light fragment will emit in the perpendicular direction to the fission axis [14–17]. However, a collinear emission of three fragments of comparable masses is also identified [23–27] in many studies and called as collinear tripartition. To estimate the most preferred A_3 fragment among all above predicted possibilities of $^{242,258}\text{Fm}$ nuclei for ECT and CCT modes of emission, the ternary fragmentation potential V (A_2) is plotted for $A_3 = 4, 30$, and 80 (or 86) fragments

in Figs. 4(a)–4(d) for both equatorial and collinear cluster tripartition. Here the ternary fragmentation potential is represented only for limited cases just for the clarity; However, the trend remains same after inclusion of in between third fragment choices. One can clearly see from Figs. 4(a) and 4(b) that the ternary fragmentation potential has smaller magnitude for $A_3 = ^4\text{He}$ case for ECT mode. The magnitude of fragmentation potential increases with increment in mass of third fragment, and hence one may conclude that the emergence of lightest third fragment is most favorable at equatorial partition of the parent nuclei. However, for CCT case, the heavier third fragments start competing the lighter ones as shown in Figs. 4(c) and 4(d) for both parent nuclei.

For further analysis, Figs. 5(a) and 5(b) represent the decay Q value (triangles) and ternary fragmentation potential V (MeV) (squares) corresponding to fragment combinations as listed in Table I of ^{242}Fm parent nucleus as a function of third fragment mass A_3 for ECT and CCT ternary emission modes. The dotted lines are used to label the minimum of potential and maximum of Q values. It is observed that the A_3 fragments like ^4He , ^8Be , ^{14}C , ^{18}O , ^{24}Ne , ^{28}Mg , ^{34}Si , ^{38}S , ^{44}Ar , ^{48}Ca , ^{54}Ti , ^{60}Cr , ^{64}Fe , ^{66}Fe , ^{70}Ni , ^{76}Zn , and ^{80}Ge have maxima in Q value and minima in the fragmenta-

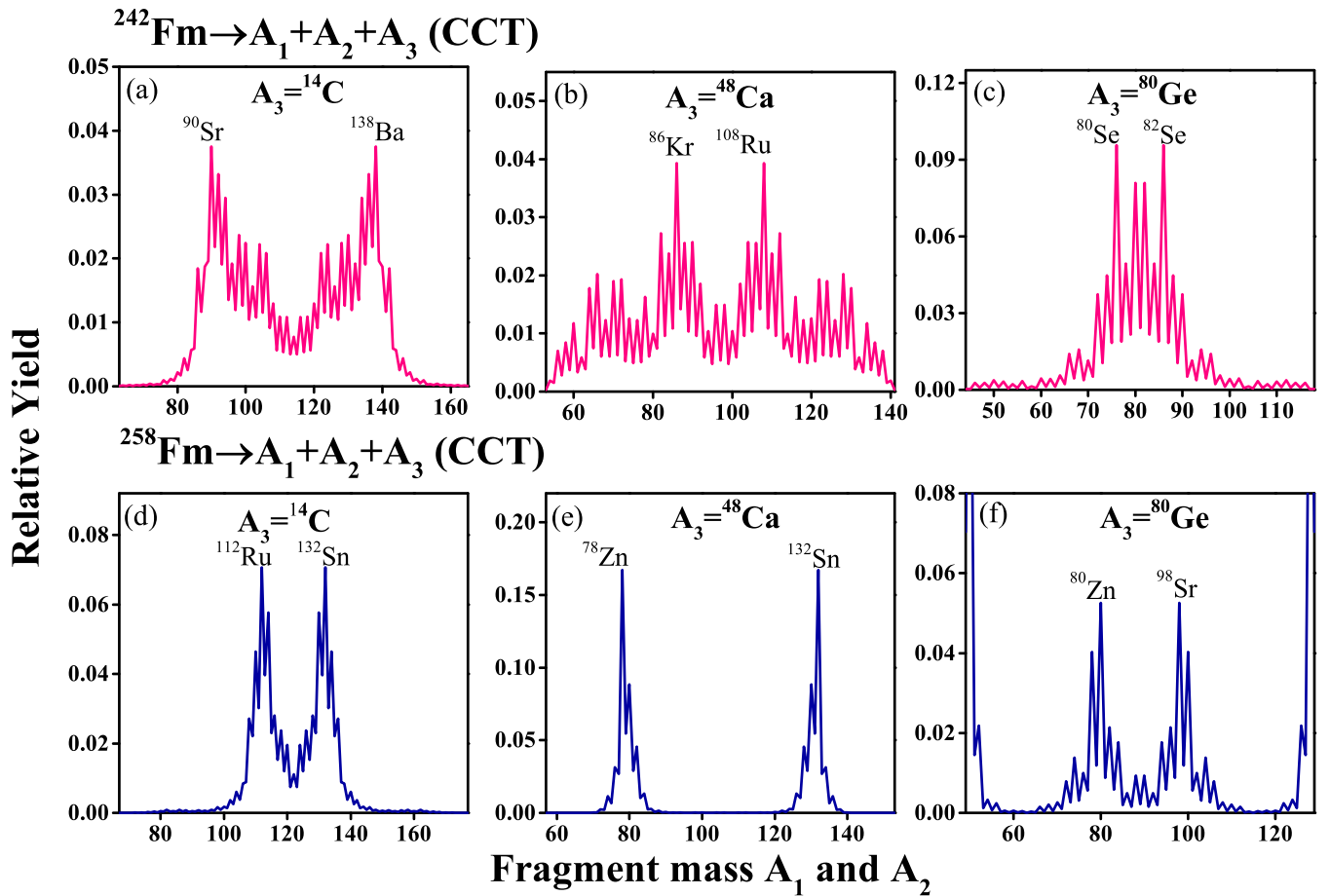


FIG. 9. The calculated relative fission yield as a function of fragment masses A_1 and A_2 for (a, b, c) ^{242}Fm and (d, e, f) ^{258}Fm for fixed A_3 fragments such as ^{14}C , ^{48}Ca , and ^{80}Ge for the CCT approach.

tion potential. Interestingly, the systematics of Q value and potential energy support the emission of even-mass third particles strongly. The fragmentation potential has higher magnitude for equatorial emission than the collinear mode particularly for heavier third fragments, for instance, it is around 40 MeV for TTF, i.e., $^{82}\text{Kr} + ^{80}\text{Se} + ^{80}\text{Ge}$, indicating that heavier third fragments have more possibility in collinear emission. The compelling reason behind this difference is the Coulomb potential because it reduces in the CCT configuration due to the large interfragment distance between A_1 and A_2 fragments, see Fig. 1(b). Moreover, this effect is large for heavy fragments due to higher charge and mass numbers. Therefore, one can say that heavy fragments and true (symmetric) ternary fission prefer the CCT emission as observed in various studies [23–27]. A deeper look of Fig. 5 supports that ^4He is the most preferred third fragment for both equatorial and collinear configurations. Similar result is observed in the experiment study of $^{256,257}\text{Fm}$ isotopes [47]. However, the potential energy of heavier fragments in CCT mode is much lower than the ECT mode, see the shaded area in the figure. This indicates that heavier third fragment starts competing the lighter third fragment in CCT mode. It is to be noted here that the ^{258}Fm has shown the same behavior as we noticed for the ^{242}Fm nucleus for both CCT and ECT configurations.

Figures 6(a)–6(c) depict the scattering potential which is calculated using $V = V_{C_{ij}} + V_{P_{ij}}$ relation as a function of separation distance (s) for three choices of third fragments such as $A_3 = ^{14}\text{C}$, ^{48}Ca , and ^{80}Ge . The scattering potential denotes the interaction between the fragments by increasing value of the surface separation s as in Eqs. (19) and (23) for ECT and CCT modes. Here in present case, we have varied the surface separation distance uniformly in ECT and CCT mode keeping the radius of corresponding fragments unchanged. The idea is to visualize the impact of variation in magnitude of surface separation distance on the barrier characteristics and also the penetration probability of the fragments emerged in these two configurations.

In the present calculations, the first turning point $s_1 = 0.4$ fm is common for all choices of third fragment for better comparison and for which the barrier penetration works. It is observed that the magnitude of barrier height is lower for CCT configuration as compared to the ECT one for each shown case. This indicates that collinear division of parent nuclei seems more preferred than the equatorial emission for the considered cases. Further, the penetrability P and relative fission yield $Y(A_i, Z_i)$ are calculated using Eqs. (13) and (15), to analyze the ternary fission fragment mass distributions of $^{242,258}\text{Fm}$ parent nuclei.

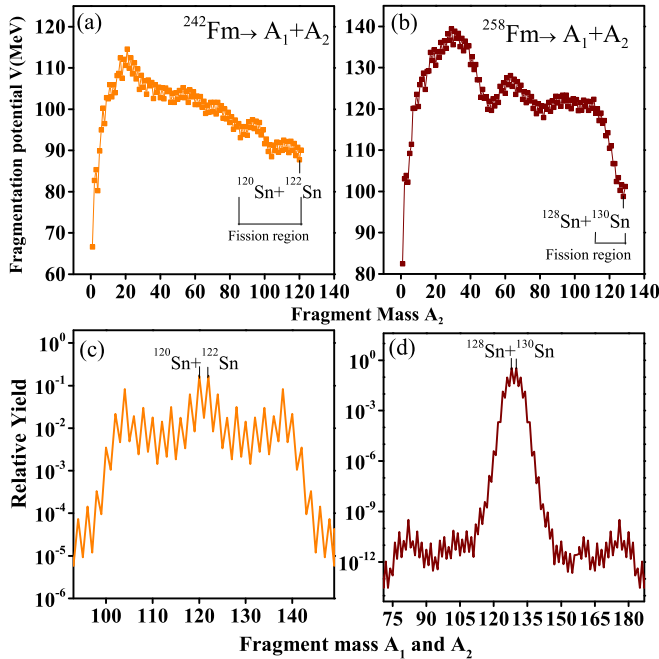


FIG. 10. The binary fragmentation potential [(a) and (b)] as a function of fragment mass A_2 and relative yield [(c) and (d)] as a function of fragment masses A_1 and A_2 using PCM for ^{242}Fm and ^{258}Fm nuclei. The most probable binary fission channel is also shown.

A relative study of barrier penetration is carried out by plotting TCM-calculated penetrability P as a function of fragment mass A_i ($i = 1, 2$) for ECT and CCT emission modes in Fig. 7 for the $A_3 = ^{48}\text{Ca}$ fragment of the ^{258}Fm nucleus. The penetration probability is higher for collinear decay mode as compared to equatorial one, because the barrier height for CCT mode is much lower than the ECT (see Fig. 6). However, in both configurations the choice of most favorable fragment combination remain same ($^{132}\text{Sn} + ^{78}\text{Zn} + ^{48}\text{Ca}$) having maximum penetrability.

Figures 8(a)–8(d) and Figs. 8(e)–8(h) represent the relative ternary fission yield of ^{242}Fm and ^{258}Fm nuclei as a function of fragment masses A_1 and A_2 for a few selected third fragments for ECT configuration. The considered A_3 fragments such as ^4He , ^{14}C , ^{48}Ca , and ^{80}Ge leaving the remaining system ($A_P - A_3$) as ^{238}Cf , ^{228}Pu , ^{194}Hg , ^{162}Er for ^{242}Fm parent nucleus, and ^{254}Cf , ^{244}Pu , ^{210}Hg , ^{178}Er , for ^{258}Fm nucleus. The lower limit of mass distribution is decided by taking 0.55 fraction of $(A_P - A_3)/2$, and higher limit is the related complementary element for each case of A_3 fragment. One may notice that the ternary fission mass distribution changes from becomes more asymmetric for heavier third fragment. However, overall distribution remains asymmetric in nature. The most probable fission fragments $A_1 + A_2$ are also marked in the figure which are same as observed across minima of fragmentation potential. Interestingly, the nature of ternary fission mass yield of these remaining nuclei, i.e., asymmetric, remain same as the binary fission mass distributions of such nuclei studied in Refs. [48–51]. Similar kind of results are observed for the CCT case as plotted in Figs. 9(a)–9(c) and

Figs. 9(d)–9(f), respectively, for ^{242}Fm and ^{258}Fm nuclei. The choice of A_1 and A_2 fragments may change as one shift from ECT to CCT configuration. Note that, the relative yield for the case of $A_3 = ^4\text{He}$ is not shown in Fig. 9 for CCT case, because the barrier potential $V(s)$ is much lower than Q value of the ^4He decay, and hence the barrier penetration is not possible.

In our previous work of binary fission of Fm isotopes [10], it was observed that mass distributions modify with increase in mass of Fm isotopes from $A_P = 242$ to 260, irrespective of deformation effects. Figures 10(a) and 10(b) represent the binary fragmentation potential for ^{242}Fm and ^{258}Fm , respectively. It is depicted from figures that for the spherical choice of fission fragments, symmetric fission is prominent for both fissioning nuclei. However, the symmetric valley becomes deeper for ^{258}Fm as compared to ^{242}Fm . Further, the relative yield of both nuclei is represented in Figs. 10(c) and 10(d), and it represents the similar result as fragmentation potential suggests. That means, the broader symmetric peak of ^{242}Fm becomes sharper for ^{258}Fm nucleus. Therefore, one can say that the binary fission prefers the symmetric distribution for considered Fm isotopes, whereas asymmetric behavior of relative mass yield is observed for the case of ternary fission. Further for the relevant discussion of binary fission, one may refer our recent paper [10], which also suggests that deformation and orientation effects play important role in binary division. In view of this, it would be of high interest to employ the deformation and orientation effect in ternary fragmentation of fissioning nuclei.

IV. SUMMARY

Summarizing, the ternary fission analysis of ^{242}Fm and ^{258}Fm isotopes is carried out within CCT and ECT configurations. Three-body fragmentation potential is used to fix the third fragment (A_3) among various possibilities. The systematics of Q value and ternary fragmentation potential support the emission of even-mass third fragments. The most probable fission channels ($A_1 + A_2 + A_3$) are identified for a wide range of light and heavy mass third fragments (1 to $A_P/3$), where A_P is mass of parent nucleus. It is observed that at least one among the three probable ternary fission fragments, associate with the neutron or proton closed shell. A relative study of equatorial and collinear emission in context of ternary fragmentation potential reveals that the light mass third fragments are equally probable for both ECT and CCT modes. However, heavier mass third fragments start competing the lighter one in collinear mode due to large interfragment distance and have lower magnitude of Coulomb potential. Further, the barrier height and barrier penetrability P are analyzed for both ECT and CCT configurations. The barrier height is observed to be lower and barrier penetrability P is higher for the CCT as compared to ECT configuration, indicating that collinear emission may be preferred over the equatorial one. Finally, a relative comparison of binary and ternary fission has been carried out in reference to fragmentation structure and relative yield. It may be of further interest to include deformation effects in the ternary fragmentation of fissioning nuclei.

ACKNOWLEDGMENT

The financial support from the UGC-DAE Consortium for Scientific Research, File No. UGC-DAE-CSR/KC/CRS/19/NP09/0920 and Department of Science

and Technology (DST), New Delhi, India in form of research project (File no. CRG/2021/001144) is gratefully acknowledged.

-
- [1] A. Allisy, *Radiat. Prot. Dosim.* **68**, 3 (1996).
- [2] H. J. Rose and G. A. Jones, *Nature (Lond.)* **307**, 245 (1984).
- [3] D. N. Poenaru, R. A. Gherghescu, and W. Greiner, *Phys. Rev. Lett.* **107**, 062503 (2011).
- [4] G. N. Flerov and K. A. Petrzhak, *Phys. Rev.* **58**, 89 (1940).
- [5] A. N. Andreyev, M. Huyse, and P. Van Duppen, *Rev. Mod. Phys.* **85**, 1541 (2013).
- [6] I. V. Ryzhov, S. G. Yavshits, G. A. Tutin, N. V. Kovalev, A. V. Saulski, N. A. Kudryashev, M. S. Onegin, L. A. Vaishnene, Y. A. Gavrikov, O. T. Grudzevich, V. D. Simutkin, S. Pomp, J. Blomgren, M. Osterlund, P. Andersson, R. Bevilacqua, J. P. Meulders, and R. Prieels, *Phys. Rev. C* **83**, 054603 (2011).
- [7] A. N. Andreyev, J. Elseviers, M. Huyse, P. VanDuppen, S. Antalic, A. Barzakh, N. Bree, T. E. Cocolios, V. F. Comas, J. Diriken, D. Fedorov, V. Fedosseev, S. Franchoo, J. A. Heredia, O. Ivanov, U. Koster, B. A. Marsh, K. Nishio, R. D. Page, N. Patronis, M. Seliverstov, I. Tsekhanovich, P. VandenBergh, J. VanDeWalle, M. Venhart, S. Vermote, M. Veselsky, C. Wagemans, T. Ichikawa, A. Iwamoto, P. Moller, and A. J. Sierk, *Phys. Rev. Lett.* **105**, 252502 (2010).
- [8] J. E. Gindler, K. F. Flynn, L. E. Glendenin, and R. K. Sjolomb, *Phys. Rev. C* **16**, 1483 (1977).
- [9] E. K. Hulet, J. F. Wild, R. J. Dougan, R. W. Lougheed, J. H. Landrum, A. D. Dougan, P. A. Baisden, C. M. Henderson, R. J. Dupzyk, R. L. Hahn, M. Schadel, K. Summerer, and G. R. Bethune, *Phys. Rev. C* **40**, 770 (1989).
- [10] A. Kaur, N. Sharma, and M. K. Sharma, *Phys. Rev. C* **103**, 034618 (2021).
- [11] L. W. Alvarez, as reported by G. Farewell, E. Segre, and C. Wiegand, *Phys. Rev.* **71**, 327 (1947).
- [12] H. Diehl and W. Greiner, *Nucl. Phys. A* **229**, 29 (1974).
- [13] M. Luis Muga, *Phys. Rev. Lett.* **11**, 129 (1963).
- [14] A. V. Ramayya *et al.*, *Nuovo Cimento A* **110**, 1073 (1997); *Phys. Rev. C* **57**, 2370 (1998).
- [15] K. Manimaran and M. Balasubramaniam, *Phys. Rev. C* **79**, 024610 (2009).
- [16] A. K. Nasirov, R. B. Tashkhodjaev, and W. von Oertzen, *Eur. Phys. J. A* **52**, 135 (2016).
- [17] A. V. Karpov, *Phys. Rev. C* **94**, 064615 (2016).
- [18] S. W. Cospser, J. Cerny, and R. C. Gatti, *Phys. Rev.* **154**, 1193 (1967).
- [19] G. M. Raisbeck and T. D. Thomas, *Phys. Rev.* **172**, 1272 (1968).
- [20] S. L. Whetstone and T. D. Thomas, *Phys. Rev. Lett.* **15**, 298 (1965); *Phys. Rev.* **154**, 1174 (1967).
- [21] D. N. Poenaru *et al.*, *Rom. Rep. Phys.* **55**, 781 (2003).
- [22] K. R. Vijayaraghavan, M. Balasubramaniam, and W. von Oertzen, *Phys. Rev. C* **91**, 044616 (2015).
- [23] R. H. Iyer and J. W. Cobble, *Phys. Rev.* **172**, 1186 (1968).
- [24] L. Rosen and A. M. Hudson, *Phys. Rev.* **78**, 533 (1950).
- [25] R. L. Fleischer, P. B. Price, R. M. Walker, and E. L. Hubbard, *Phys. Rev.* **143**, 943 (1966).
- [26] V. P. Pereygin, N. H. Shadieva, S. P. Tretyakova, A. H. Boos, and R. Brandt, *Nucl. Phys. A* **127**, 577 (1969).
- [27] H. J. Becker, P. Vater, R. Brandt, and A. H. Boos, *Phys. Lett. B* **50**, 445 (1974).
- [28] S. Thakur *et al.*, *Int. J. Mod. Phys. E* **22**, 1350014 (2013).
- [29] K. Manimaran and M. Balasubramaniam, *Phys. Rev. C* **83**, 034609 (2011).
- [30] J. Maruhn and W. Greiner, *Phys. Rev. Lett.* **32**, 548 (1974).
- [31] R. K. Gupta, W. Scheid, and W. Greiner, *Phys. Rev. Lett.* **35**, 353 (1975).
- [32] R. K. Gupta, A. Sandulescu, and W. Greiner, *Phys. Lett. B* **67**, 257 (1977).
- [33] N. Sharma, A. Kaur, and M. K. Sharma, *Phys. Rev. C* **102**, 064603 (2020).
- [34] K. Sharma, G. Sawhney, and M. K. Sharma, *Phys. Rev. C* **96**, 054307 (2017).
- [35] G. Audi and A. H. Wapstra, *Nucl. Phys. A* **595**, 409 (1995).
- [36] P. Möller, J. R. Nix, W. D. Myers, and W. J. Swiatecki, *At. Nucl. Data Tables* **59**, 185 (1995).
- [37] W. D. Myers and W. J. Swiatecki, *Phys. Rev. C* **62**, 044610 (2000).
- [38] I. Dutt and R. K. Puri, *Phys. Rev. C* **81**, 064609 (2010).
- [39] K. R. Vijayaraghavan, M. Balasubramaniam, and W. von Oertzen, *Eur. Phys. J. A* **48**, 27 (2012).
- [40] R. B. Tashkhodjaev, A. I. Muminov, A. K. Nasirov, W. von Oertzen, and Y. Oh, *Phys. Rev. C* **91**, 054612 (2015).
- [41] W. von Oertzen and A. K. Nasirov, *J. Phys. Conf. Ser.* **569**, 012040 (2014).
- [42] A. Algora, J. Cesh, J. Darai, and P. O. Hess, *Phys. Lett. B* **639**, 451 (2006).
- [43] Yu V. Pyaktov *et al.*, *Rom. Rep. Phys.* **59**, 569 (2007).
- [44] R. K. Gupta and W. Griener, *Int. J. Mod. Phys. E* **03**, 335 (1994).
- [45] R. Bonetti and A. Gugliemetti, *Rom. Rep. Phys.* **59**, 301 (2007).
- [46] Yu. V. Pyatkov *et al.*, *Eur. Phys. J. A* **45**, 29 (2010).
- [47] J. F. Wild, P. A. Baisden, R. J. Dougan, E. K. Hulet, R. W. Lougheed, and J. H. Landrum, *Phys. Rev. C* **32**, 488 (1985).
- [48] A. V. Andreev, G. G. Adamian, N. V. Antonenko, and A. N. Andreyev, *Phys. Rev. C* **88**, 047604 (2013).
- [49] H. Pasca, A. V. Andreev, G. G. Adamian, and N. V. Antonenko, *Phys. Rev. C* **99**, 064611 (2019).
- [50] K. Sharma, G. Sawhney, Manoj K. Sharma, and R. K. Gupta, *Nucl. Phys. A* **972**, 1 (2018).
- [51] N. K. Virk, R. Kumar, and M. K. Sharma, *Int. J. Mod. Phys. E* **30**, 2150001 (2021).